Macromolecules

Article

pubs.acs.org/Macromolecules

Helical Phase Driven by Solvent Evaporation in Self-Assembly of Poly(4-vinylpyridine)-*block*-poly(L-lactide) Chiral Block Copolymers

Tsai-Ming Chung,[†] Hsiao-Fang Wang,[†] Tao Lin,[†] Yeo-Wan Chiang,*[,§] Yi-Chun Chen,[∥] Bao-Tsan Ko,*[,⊥] and Rong-Ming Ho*[,†,‡,#]

[†]Department of Chemical Engineering, National Tsing Hua University, Hsinchu 30013, Taiwan

[‡]Institute of NanoEngineering and MicroSystems, National Tsing Hua University, Hsinchu 30013, Taiwan

[§]Department of Materials and Optoelectronic Science, Center for Nanoscience and Nanotechnology, National Sun Yat-Sen University, Kaohsiung 80424, Taiwan

[∥]Material and Chemical Research Laboratories, Industrial Technology Research Institute, Hsinchu 310, Taiwan

[⊥]Department of Chemistry, Chung Yuan Christian University, Chung Li 32023, Taiwan

[#]Frontier Research Center on Fundamental and Applied Sciences of Matters, National Tsing Hua University, Hsinchu, 30013, Taiwan

Supporting Information

ABSTRACT: A series of chiral block copolymers (BCPs*), poly(4-vinylpyridine)-*block*-poly(L-lactide) (P4VP−PLLA), are synthesized through atom transfer radical polymerization and living ring-opening polymerization. Except for typical microphase-separated phases, such as lamellae (L) and hexagonally packed cylinders (HC), a helical phase (H*) with hexagonally packed PLLA helices in a P4VP matrix can be found in the self-assembly of P4VP−PLLA BCPs*, reflecting the chirality effect on BCP self-assembly. The H* formation is strongly dependent upon the solvent evaporation rate for solution casting at which fast evaporation gives the H* phase and slow evaporation results in the HC phase. To further examine the metastability of the H* phase associated with the dynamics of BCP* chains during self-assembly, P4VP−PLLA BCPs* having different molecular weights at a constant composition are utilized for self-assembly. Under the same evaporation rate for solution casting, the H* phase can be obtained in high-molecular-weight P4VP−PLLA BCP* whereas a stable HC phase is found in low-molecular-weight P4VP−PLLA BCP*, indicating the kinetic origin of H* formation due to the long and highly entangled chains in solution for self-assembly. Consequently, the H* phase can be driven by solvent evaporation through a kinetically trapped process and is regarded as a long-lived metastable phase.

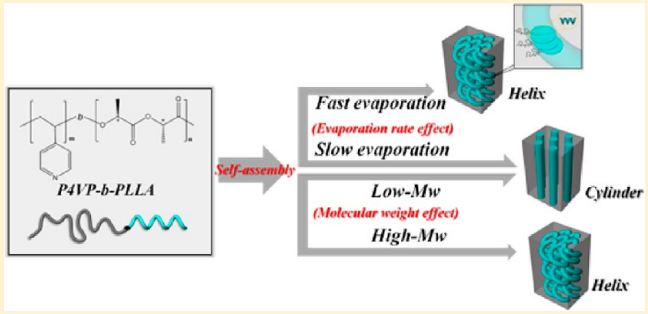

INTRODUCTION

Because of the miscellaneous diversity of helical morphologies in nature, the formation mechanism of the helical morphology has been extensively investigated in many research fields such as biochemistry, supramolecular chemistry, and polymer science. Biomimicking from nature, the helical structures having different length scales have been found by the interplay of noncovalent bonding interactions (that is, the control of secondary forces).[1−7] Block copolymers (BCPs) consisting of chemically different components are able to self-assemble into various ordered nanostructures, such as body-centered cubic spheres (BCC), hexagonally packed cylinders (HC), gyroid (G), and lamellae (L), as a consequence of the incompatibility of the constituent blocks.[8,9] Recently, a new phase, a helical phase (H*) comprising hexagonally packed PLLA helices in a PS matrix in three dimensions, was found in the self-assembly of polystyrene-*block*-poly(L-lactide) (PS−PLLA) BCPs.[10−19] The formation of the H* phase is attributed to the chirality effect on the self-assembly of BCP so that this BCP having chiral segments was named as a chiral BCP (denoted as BCP*). The corresponding phase diagram of the PS−PLLA BCP* demonstrates that the H* formation is strongly dependent upon the overall molecular weight and composition, showing that the H* phase is apparently obtained in the high-molecular-weight region.[13] Moreover, through a thermal annealing process, interesting phase transitions from the H* to stable HC and G phases could be found in the BCP* self-assembly.[15] As a result, the H* formation is referred to slow kinetics associated with long and highly entangled chains for self-assembly. Namely, the H* phase is attributed to a kinetically trapped process due to the prolonged relaxation time. Consequently, the H* phase is regarded as a long-lived metastable state.[13]

Received: October 15, 2012
Revised: December 3, 2012
Published: December 11, 2012

ACS Publications © 2012 American Chemical Society

dx.doi.org/10.1021/ma302159p | *Macromolecules* 2012, 45, 9727−9733

Scheme 1. Synthetic Routes of P4VP−PLLA BCPs*

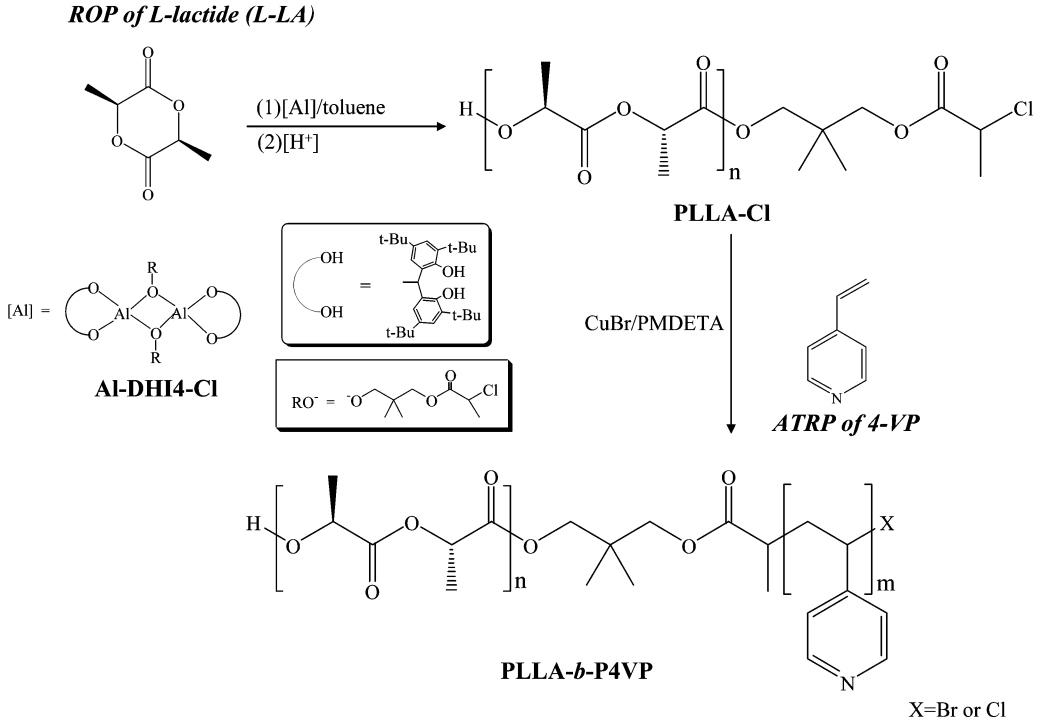

Table 1. Characterization of Representative P4VP−PLLA BCPs*

code	$M_{n,P4VP}$ (kg/mol)[a]	$M_{n,PLLA}$ (kg/mol)[a]	$M_{n,total}$ (kg/mol)	M_w/M_n[b]	f_{PLLA}^{v}	morphology
P4VP13-PLLA11	13.2	10.5	23.7	1.24	0.42	L
P4VP16-PLLA05	15.5	5.4	20.9	1.17	0.23	H*
P4VP28-PLLA09	27.7	9.2	36.9	1.21	0.22	H*
P4VP19-PLLA05	18.9	5.4	24.3	1.10	0.20	HC

[a] $M_{n,P4VP}$ and $M_{n,PLLA}$ were characterized by proton nuclear magnetic resonance (^{1}H NMR). [b] Polydispersity index (M_w/M_n) was determined by gel permeation chromatography (GPC) by using standard calibration. All samples were prepared by solution casting from dichloromethane solution (10 wt %).

In this study, the chirality effect on the self-assembly of BCPs* is further examined by synthesizing a series of poly(4-vinylpyridine)-*block*-poly(L-lactide) (P4VP−PLLA) BCPs* in comparison with the PS−PLLA BCPs*. Moreover, in contrast to the phase transitions through a thermal annealing process, the P4VP−PLLA BCP* samples are prepared through a solution cast process by controlling the solvent evaporation rate so as to examine the formation mechanism and the metastability of the H* phase associated with the dynamics of BCP* chains during self-assembly. Also, P4VP−PLLA BCPs* having different molecular weights at a constant composition are utilized to investigate the effect of the BCP* relaxation time on the kinetically driven H* phase formation.

EXPERIMENTAL SECTION

Synthesis and Characterization of P4VP−PLLA BCPs*. A series of poly(4-vinylpyridine)-*b*-poly(L-lactide) (P4VP−PLLA) diblock copolymers were synthesized by atom transfer radical polymerization (ATRP) and living ring-opening polymerization (ROP) using a double-headed initiator, DHI4-Cl (Scheme 1).[20] To prepare a chloride-terminated poly(L-lactide) (PLLA-Cl), ROP of L-lactide catalyzed by Al-DHI4-Cl in the presence of DHI4-Cl as the chain transfer agent was performed, and the produced PLLA-Cls with different molecular weights (M_n = 5400−10 500 g/mol) are listed in Table 1. P4VP−PLLA block copolymers were synthesized by ATRP of 4-vinylpyridine (4-VP) from PLLA-Cl in the presence of CuBr/PMDETA catalysts.[21] The ^{1}H NMR spectrum of P4VP−PLLA reveals the successful polymerization of 4-VP, and the synthesized samples show unimodal GPC curves (PDI < 1.25) shifting to high molecular weight in comparison to the macroinitiator, PLLA-Cl. Estimation of the relative compositions of block copolymers was calculated from the integration of the methine protons at 5.14 ppm of the PLLA block and that of the pyridine protons of P4VP block at 8.31 ppm. Detailed synthetic procedures are described in the Supporting Information. A series of the P4VP−PLLA block copolymers utilized in this study are listed in Table 1. Based on the molecular weight and volume fraction, the P4VP−PLLA BCPs* were assigned as P4VPx−PLLAy ($f_{PLLA}^{v} = z$) in which x and y represent the molecular weight (base = 1000 kg/mol) of P4VP and PLLA blocks, respectively, and z is the volume fraction of the P4VP block by assuming that the densities of P4VP and PLLA are 0.998 and 1.248 g/cm^3, respectively (Table 1).

Materials. A variety of the PS−PLLA solutions (10 wt %) were first placed into glass bottles sealed with aluminum foils. A hole (0.8 mm in diameter) was punched on the center of the aluminum foil to let the solvent evaporate. From the weight loss of the solution, the drying time and the amounts of the residual solvents can be estimated. To avoid the solvent retaining in the as-cast sample, the drying time was largely extended. As the as-cast samples were completed vitrified, the vitrified samples were subsequently placed into a vacuum oven for further drying.

Transmission Electron Microscopy (TEM). Samples were first microtomed by ultramicrotomy (thickness ~50 nm) at room temperature and then stained by exposing the microsections to the vapor of a 4% aqueous RuO_4 solution for TEM observation. Bright-

dx.doi.org/10.1021/ma302159p | Macromolecules 2012, 45, 9727−9733

field TEM images were obtained on a JEOL JEM-2100 TEM at an accelerating voltage of 200 kV. After staining by RuO_4 vapor, the PLLA microdomains appeared bright and the P4VP appeared dark.

X-ray Experiments. Small-angle X-ray scattering (SAXS) experiments were conducted at the synchrotron X-ray beamline X27C at the National Synchrotron Light Source (NSLS) in Brookhaven National Laboratory (BNL) and at synchrotron X-ray beamline 23A1 at the National Synchrotron Research Center (NSRRC) in Taiwan. The wavelength of the X-ray beam was 0.1371 nm. A MAR CCD X-ray detector (MAR USA) was applied to collect the 2D SAXS patterns. The scattering angle of the SAXS pattern was calibrated using silver behenate, with the first-order scattering vector q^* ($q^* = 4\pi\lambda^{-1} \sin\theta$, where 2θ is the scattering angle) of 1.076 nm^{-1}.

RESULTS AND DISCUSSION

Microphase-Separated Phases. Bulk samples of the P4VP−PLLA BCPs* with various compositions ranging from 0.2 to 0.42 were prepared by solution casting from a dichloromethane (a neutral solvent) solution (10 wt %) at room temperature and then dried in a vacuum oven at 65 °C for 3 days. After quenching from microphase-separated melt at 175 °C for 3 min, the thermally treated P4VP−PLLA samples were subsequently sectioned by ultramicrotome. A variety of self-assembled nanostructures associated with composition and overall molecular weight can be observed by TEM (Figure 1).

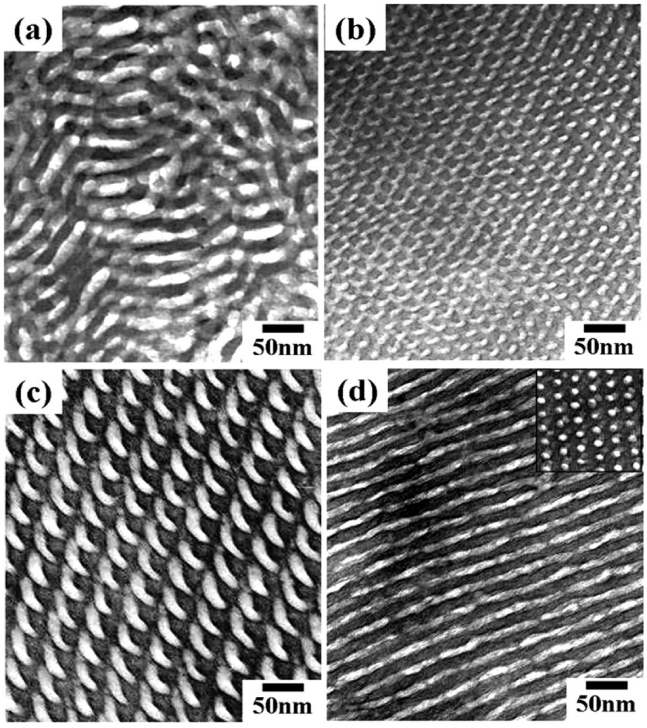

Figure 1. TEM micrographs of (a) P4VP13−PLLA11 (f_{PLLA}^{ν} = 0.42), (b) P4VP16−PLLA05 (f_{PLLA}^{ν} = 0.23), (c) P4VP28−PLLA09 (f_{PLLA}^{ν} = 0.22), and (d) P4VP19−PLLA05 (f_{PLLA}^{ν} = 0.20). After RuO_4 staining, the dark region represents the P4VP microdomain and the bright region is the PLLA microdomain.

Well-defined microphase-separated lamellar morphology can be found in the P4VP13−PLLA11 (f_{PLLA}^{ν} = 0.42) BCP* at which the P4VP microdomains appear dark due to RuO_4 staining and the bright regions are the PLLA microdomains (Figure 1a). Consistently, the corresponding one-dimensional (1-D) SAXS profile shows that the reflections occur at q^* ratios of 1:2:3:4 (Figure 2a). With increasing the degree of compositional

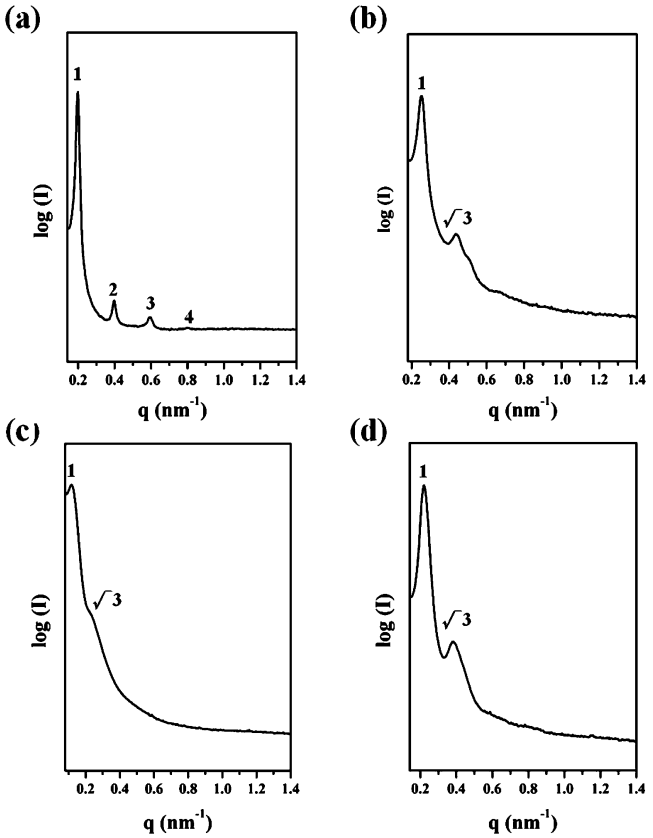

Figure 2. 1-D SAXS profiles of solution-cast samples after quenching from the microphase-separated melt: (a) P4VP13−PLLA11 (f_{PLLA}^{ν} = 0.42), (b) P4VP16−PLLA05 (f_{PLLA}^{ν} = 0.23), (c) P4VP28−PLLA09 (f_{PLLA}^{ν} = 0.22), and (d) P4VP19−PLLA05 (f_{PLLA}^{ν} = 0.20).

asymmetry, various microphase-separated phases can be found. A helical texture (namely, a helical phase (H*)) having crescent-like projection images can be found in the P4VP16−PLLA05 (f_{PLLA}^{ν} = 0.23) and P4VP28−PLLA09 (f_{PLLA}^{ν} = 0.22) BCPs* (Figure 1b,c). According to the characterization of the H* phase, this crescent-like morphology is the unique character of the H* phase associated with the microsection thickness for projection.[13] The corresponding 1-D SAXS profile consisting of the reflections at q^* ratio of $1:\sqrt{3}$ indicates the hexagonally packed structure, i.e., hexagonally packed PLLA helices in a P4VP matrix (Figure 2b,c). Notably, as the increase of the overall molecular weight at a constant volume fraction, the PLLA helices exhibit thicker thickness in the P4VP28−PLLA09 (f_{PLLA}^{ν} = 0.22) than that in the P4VP16−PLLA05 (f_{PLLA}^{ν} = 0.23) under TEM observation. Consistently, the SAXS profiles show that the long period of P4VP28−PLLA09 (f_{PLLA}^{ν} = 0.22) (54.6 nm) is much larger than that of P4VP16−PLLA05 (f_{PLLA}^{ν} = 0.23) (26.2 nm). Interestingly, as f_{PLLA}^{ν} = 0.20 in the P4VP19−PLLA05 BCP*, cylindrical textures along longitudinal and lateral directions can be observed (Figure 1d), indicating the formation of PLLA cylinders in a P4VP matrix. Also, the hexagonal arrangement of the cylinders can be identified by the 1-D SAXS profile in which the reflections occur at the q^* ratio of $1:\sqrt{3}$ (Figure 2d), confirming the formation of the HC phase.

As reported previously,[10−19] the formation of H* phase can be successfully induced by the transfer of chirality from molecular chirality into phase chirality in the self-assembly of the PS−PLLA BCPs*, reflecting the formation of helical

dx.doi.org/10.1021/ma302159p | Macromolecules 2012, 45, 9727−9733

morphologies with different length scales driven by the chirality effect for BCP self-assembly. Interestingly, on the basis of the phase behaviors of PS−PLLA and PV4P−PLLA BCPs*, the composition effect on the formation of H* phase in the P4VP−PLLA BCPs* is obviously different than that in PS−PLLA BCPs*.[13] By comparison, the phase boundary for the H* formation is in between 0.22 and 0.2 of f_{PLLA}^{v} in the P4VP−PLLA BCPs*, whereas the H* phase is obtained in the PS−PLLA BCPs* as f_{PLLA}^{v} is larger than 0.3. We speculate that this discrepancy might be attributed to the difference in conformational asymmetry between these two systems. As reported previously,[22] the shift of phase boundary in the BCP phase diagram of an A−B diblock copolymer is strongly affected by the ratio of the A and B statistical segment lengths, a_A/a_B. According to the statistical segment lengths of the P4VP (7.97 nm), PS (6.81 nm), and PLLA (10.0 nm),[23,24] the ratio of the P4VP and PLLA statistical segment lengths, $a_{P4VP}/a_{PLLA} = 0.80$, is significantly different than the ratio of the PS and PLLA statistical segment lengths, $a_{PS}/a_{PLLA} = 0.68$. This obvious discrepancy in the ratio of statistical segment lengths might give rise to an enhancement in the difference of conformational asymmetry between the P4VP−PLLA and PS−PLLA BCP*, resulting in the dissimilar phase boundary in these two systems. Also, the difference in the conformational asymmetry might lead to the change of the metastability of the microphase-separated phases in the BCP* phase diagram. Moreover, in accordance with the BCP thermodynamics, the phase behavior is also strongly affected by the segregation strength χN (the product of interaction parameter and degree of the polymerization). Based on the phase behaviors of PS−PLLA and P4VP−PLLA, the formation of the H* is indeed dependent upon the segregation strength χN. Note that the interaction parameter is also correlated with the statistical segment lengths of constituted blocks. As a result, we speculate that the differences in the phase diagrams of the P4VP−PLLA and the PS−PLLA are attributed to the effect of segregation strength resulting from the variation on constituted statistical segment lengths. Systematic studies associated with the segregation strength on the phase diagram, phase stability, and phase transitions in the self-assembly of the BCPs* are still under investigation.

H* Driven by Solvent Evaporation. Our previous results indicate that the H* formation is attributed to a kinetically trapped process because of the prolonged relaxation time of polymer chains.[13] Phase transitions from the metastable H* to stable G or HC phases can be driven by thermal annealing.[11,13,15] In contrast to thermo-driven BCP phase transition, a process through solvent-induced phase transition can easily avoid the problem of thermal degradation and may largely increase the chain mobility to give an efficient method to track the structural and morphological evolution during phase transitions. Accordingly, a series of self-assembled morphologies in the P4VP−PLLA BCP* were then prepared by controlling the evaporation rate for solution casting so as to explore the phase transitions associated with the dynamics of BCP* chains during self-assembly (i.e., the chain mobility for self-assembly). In general, the formation of BCP microphase separation is strongly affected by the evaporation rate for solution casting.[25] For instance, fast evaporation rate for solution casting may cause a short time period for self-assembly and results in a disorder morphology (i.e., unstable phase) with randomly distributed microdomains after casting. By contrast, slow evaporation may give well-defined microphase-separated morphologies (i.e., thermodynamically stable phases) because of a prolonged time period for self-assembly. Consequently, by controlling the evaporation rate for solution casting, the kinetically trapped process can be carried out to acquire metastable phases such as H* having local minimum in Gibbs free energy.

A variety of good solvents, including dichloromethane (CH_2Cl_2), chloroform ($CHCl_3$), 1,2-dichloroethane ($C_2H_4Cl_2$), and 1,1,2-trichloroethane ($C_2H_3Cl_3$), were utilized to perform solution casting at different evaporation rate. The P4VP16−PLLA05 ($f_{PLLA}^{v} = 0.23$) BCP* was first dissolved in dichloromethane, and then the solution were isothermally treated at 35 °C for solution casting (vapor pressure of dichloromethane is 642 mmHg at 35 °C, denoted as $V_{CH_2Cl_2}^{35\ °C} = 642$ mmHg). After 12 h, the solution was completely dried, and then P4VP16−PLLA05 ($f_{PLLA}^{v} = 0.23$) bulk sample was obtained. The unique crescent-like projection image under TEM observations (Figure 3a) and hexagonally

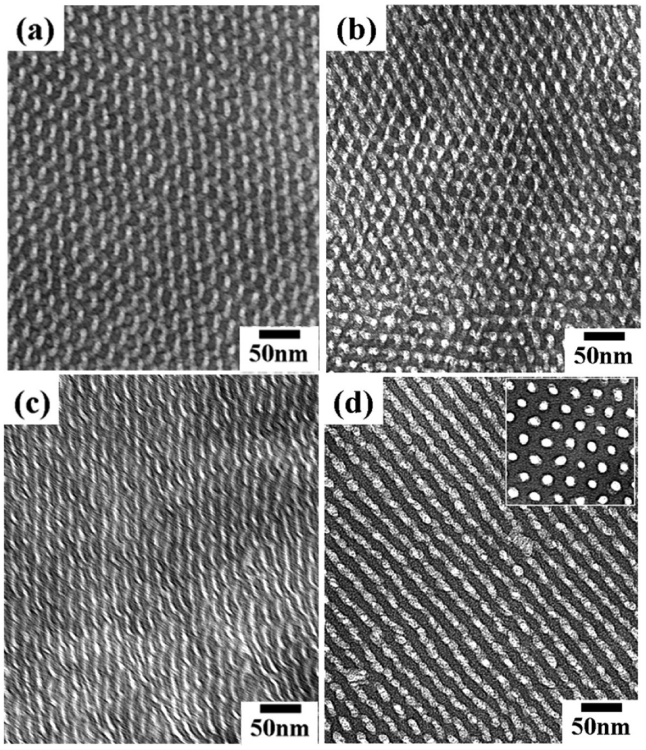

Figure 3. TEM micrographs of solution-cast P4VP16−PLLA05 ($f_{PLLA}^{v} = 0.23$) samples by using various solvents: (a) dichloromethane ($V_{CH_2Cl_2}^{35\ °C} = 642$ mmHg); (b) dichloromethane ($V_{CH_2Cl_2}^{20\ °C} = 342$ mmHg); (c) chloroform ($V_{CHCl_3}^{20\ °C} = 159.6$ mmHg); (d) 1,2-dichloroethane ($V_{C_2H_4Cl_2}^{20\ °C} = 61$ mmHg). The micrograph in the inset of (d) is the projection image along longitudinal direction of the PLLA cylinder.

packed structure as evidenced by 1D SAXS profile (Figure 4a) suggest the formation of the H* phase in the P4VP16−PLLA05 ($f_{PLLA}^{v} = 0.23$) BCP*. Namely, the metastable H* phase can be obtained under this evaporation condition. To further examine the kinetics of the H* formation, an extension of the self-assembled time period to 24 h was carried out by decreasing the evaporation temperature from 35 to 20 °C for solution casting ($V_{CH_2Cl_2}^{20\ °C} = 342$ mmHg). The TEM micrograph (Figure 3b) shows a similar projection image to the

dx.doi.org/10.1021/ma302159p | Macromolecules 2012, 45, 9727−9733

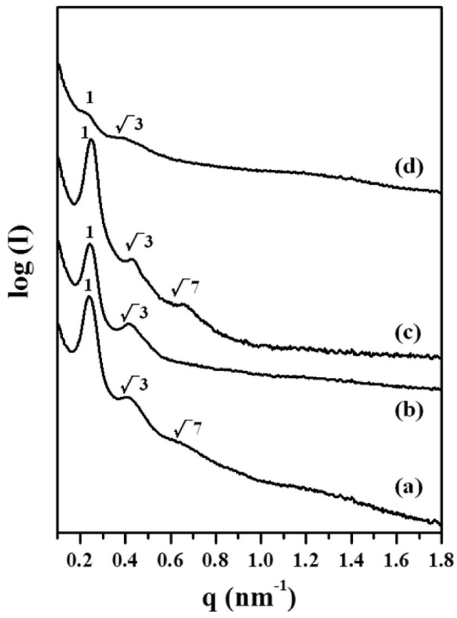

Figure 4. 1-D SAXS profiles of solution-cast P4VP16−PLLA05 (f_{PLLA}^{v} = 0.23) bulk samples by using various solvents: (a) dichloromethane ($V_{CH_2Cl_2}^{35\ °C}$ = 642 mmHg); (b) dichloromethane ($V_{CH_2Cl_2}^{20\ °C}$ = 342 mmHg); (c) chloroform ($V_{CHCl_3}^{20\ °C}$ = 159.6 mmHg); (d) 1,2-dichloroethane ($V_{C_2H_4Cl_2}^{20\ °C}$ = 61 mmHg).

preobserved H* phase (Figure 3a). The corresponding 1-D SAXS profile further confirms the hexagonally packed PLLA helices in the P4VP matrix (Figure 4b). Interestingly, with further extending the time period for self-assembly by using chloroform as a solvent for solution casting at 20 °C ($V_{CHCl_3}^{20\ °C}$ = 159.6 mmHg), the TEM micrograph (Figure 3c) exhibits a helix-like morphology (i.e., intermediate state) having more stretched and elongated curvature along the helical axis. Notably, the corresponding 1-D SAXS profile exhibits an obvious decrease in the scattering intensity for the high-order reflections (Figure 4c). We speculate that the slow evaporation of the chloroform for solution casting might result in a tendency to form a stable morphology (namely, an HC phase). Owing to the incoherence of the morphological evolution from the H* phase to HC phase in different monograins, long-range order of the microphase-separated helices might be diminished after phase transition.[12]

To fully develop a stable morphology in the self-assembly of the P4VP−PLLA BCPs*, a slow self-assembled process was thus carried out by using 1,2-dichloroethane as a solvent for solution casting ($V_{C_2H_4Cl_2}^{20\ °C}$ = 61 mmHg). Through this slow evaporation process, instead of the H* formation, the microphase-separated phase of the P4VP16−PLLA05 BCP* exhibits an HC phase in which the collimated and hexagonally packed cylinders can be observed along lateral and longitudinal direction, respectively (Figure 3d). Similarly, because of the full development of the HC phase from the phase transition of the H* phase, a decrease in the scattering intensity of the reflections can be found due to the incoherence of the phase transitions from different monograins (Figure 4d) as described above. Moreover, under an extremely slow evaporation condition, PLLA crystallization might dominate the self-assembled morphology and interrupt BCP microphase separation. Accordingly, in the case of the extremely long time period for self-assembly, BCP microphase separation might inevitably be overwhelmed by the crystallization of PLLA blocks. As a result, by controlling the evaporation rate for solution casting (i.e., manipulating the time period for self-assembly), the metastable H* phase and stable HC phases can be obtained in the P4VP−PLLA BCP* under fast and slow evaporation conditions, respectively.

Molecular Weight Effect. Except for the self-assembled time period, the chain mobility, which is strongly dependent upon molecular weight, also plays an important role in the kinetics of BCP self-assembly, especially for the formation of metastable phases from microphase separation. To explore the molecular weight effect on the morphological evolution from solution casting, a high-molecular-weight P4VP−PLLA BCP*, P4VP28−PLLA09 (f_{PLLA}^{v} = 0.22) BCP*, was utilized for self-assembly. As shown in Figure 5a, the TEM micrograph of the

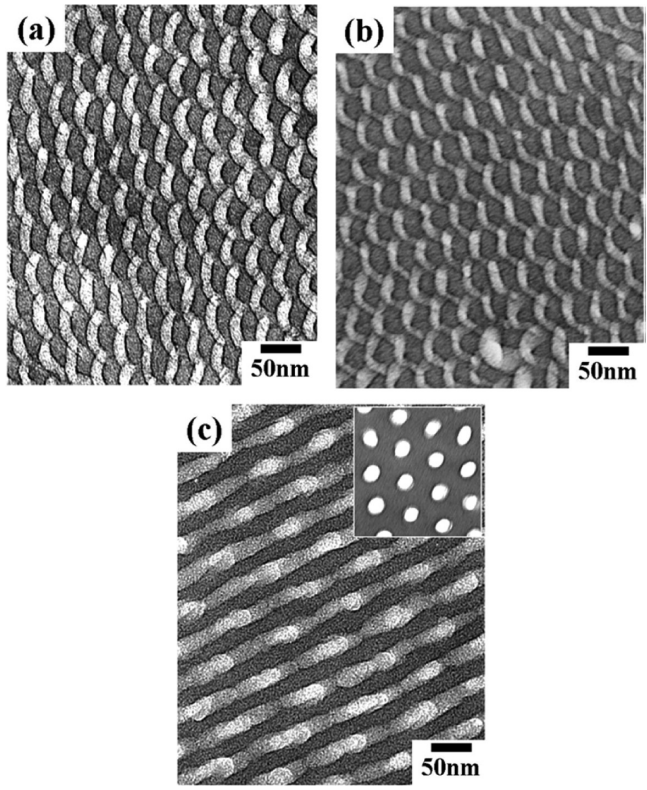

Figure 5. TEM micrographs of solution-cast P4VP28−PLLA09 (f_{PLLA}^{v} = 0.22) samples by using various solvents: (a) dichloromethane ($V_{CH_2Cl_2}^{35\ °C}$ = 642 mmHg); (b) 1,2-dichloroethane ($V_{C_2H_4Cl_2}^{20\ °C}$ = 61 mmHg); (c) 1,1,2-trichloroethane ($V_{C_2H_3Cl_3}^{20\ °C}$ = 17.1 mmHg). The micrograph in the inset of (c) is along longitudinal direction of the PLLA cylinder.

solution-cast P4VP28−PLLA09 (f_{PLLA}^{v} = 0.22) BCP* from dichloromethane at 35 °C presents a distinct H* morphology. Interestingly, instead of forming an HC phase in the low-molecular-weight P4VP16−PLLA05 (f_{PLLA}^{v} = 0.23) BCP* (Figure 3a), the H* phase formed in the high-molecular-weight P4VP28−PLLA09 (f_{PLLA}^{v} = 0.22) BCP* under a very slow evaporation condition by using 1,2-dichloroethane as a solvent for solution casting at 20 °C ($V_{C_2H_4Cl_2}^{20\ °C}$ = 61 mmHg). This indicates that the kinetically trapped effect can be significantly enhanced in a high-molecular-weight BCP* than in a low-molecular-weight BCP*, leading to the formation of the H*

dx.doi.org/10.1021/ma302159p | Macromolecules 2012, 45, 9727−9733

phase. Accordingly, to acquire a stable phase from the self-assembly of this high-molecular-weight sample, an extremely slow evaporation rate should be carried out so that the solution casting is conducted by using 1,1,2-tricholoethane as a solvent ($V_{C_2H_3Cl_3}^{20\ °C}$ = 17.1 mmHg). As shown in Figure 5c, a stable HC phase can be obtained under TEM in the as-cast high-molecular-weight P4VP28−PLLA09 (f_{PLLA}^{v} = 0.22) BCP* from 1,1,2-trichloroethane at 20 °C. Therefore, as the increase of the BCP* molecular weight (namely, the decrease of the BCP* chain mobility), the enhancement in the relaxation time of the BCP* chains may give higher tendency to induce the formation of the metastable H* phase. This indicates that the H* formation is truly attributed to the kinetic origin associated with long and highly entangled chains.

CONCLUSIONS

Similar to the PS−PLLA BCPs*, the H* phase can be successfully fabricated in the self-assembly of P4VP−PLLA BCPs*, demonstrating that the chirality effect on the self-assembly of BCPs* is applicable and promising for the design of a phase with helical sense. By controlling the solvent evaporation rate for solution casting, that is, manipulating the time period for self-assembly, the formations of the metastable H* phase, helix-like morphology, and stable HC phase can be obtained, indicating that the H* phase is a consequence of kinetically trapped process. Also, in contrast to a stable HC phase in the low-molecular-weight P4VP−PLLA BCP*, the H* phase still remains in the high-molecular-weight P4VP−PLLA BCP* under the same evaporation condition. This indicates that the kinetically trapped effect can be effectively enhanced by the increase of the BCP* molecular weight, further demonstrating that the H* phase is a long-lived metastable phase. As a result, the metastable H* phase can be successfully driven by reducing self-assembled time period via the reduction of the evaporation rate for solution casting and/or by increasing the relaxation time of the BCP* chains via the increase of the overall molecular weight of BCP*. This provides an efficient way with less degradable problem for acquiring a phase with helical sense.

ASSOCIATED CONTENT

Supporting Information

Detailed synthetic procedures for P4VP−PLLA BCPs*; Table S1 for the P4VP−PLLA BCPs* with various compositions; TEM micrographs of P4VP23−PLLA09 (f_{PLLA}^{v} = 0.25), P4VP12−PLLA06 (f_{PLLA}^{v} = 0.29), and P4VP15−PLLA09 (f_{PLLA}^{v} = 0.33); WAXD patterns of as-cast P4VP−PLLA samples from dichloromethane and PLLA homopolymer; TEM micrographs of solution-cast P4VP16−PLLA05 (f_{PLLA}^{v} = 0.23) from dichloromethane ($V_{CH_2Cl_2}^{25\ °C}$ = 342 mmHg) solution at 25 °C before and after long-time annealing at 110 °C; TGA heating curve of solution-cast P4VP19−PLLA05 (f^{v}_{PLLA} = 0.23) from 1,2-dichloroethane ($V_{C_2H_4Cl_2}^{20\ °C}$ = 61 mmHg) solution at 20 °C. This material is available free of charge via the Internet at http://pubs.acs.org.

AUTHOR INFORMATION

Corresponding Author

*Tel +886-3-5738349; Fax +886-3-5715408; e-mail rmho@mx.nthu.edu.tw.

Notes

The authors declare no competing financial interest.

ACKNOWLEDGMENTS

Authors thank Dr. L. Rong of National Synchrotron Light Source at Brookhaven National Laboratory (USA) and Drs. U.-S. Jeng of National Synchrotron Radiation Research Center (Taiwan) for their help in synchrotron SAXS experiments. We also thank Dr. S. Z. D. Cheng of Institute of Polymer Science of University of Akron and Dr. E. L. Thomas of Department of Mechanical Engineering and Materials Science of University of Rice for their helpful discussions. Authors appreciate the National Science Council of the Republic of China (100-2120-M-007-013), Taiwan, for financially supporting this research.

REFERENCES

(1) Nelson, J. C.; Saven, J. G.; Moore, J. S.; Wolynes, P. G. *Science* **1997**, *277*, 1793−1796.
(2) Cornelissen, J. J. L. M.; Fischer, M.; Sommerdijk, N. A. J. M.; Nolte, R. J. M. *Science* **1998**, *280*, 1427−1430.
(3) Engelkamp, H.; Middelbeek, S.; Nolte, R. J. M. *Science* **1999**, *284*, 785−788.
(4) Orr, G. W.; Barbour, L. J.; Atwood, J. L. *Science* **1999**, *285*, 1049−1052.
(5) Li, C. Y.; Cheng, S. Z. D.; Ge, J. J.; Bai, F.; Zhang, J. Z.; Mann, I. K.; Harris, F. W.; Chien, L.-C.; Yan, D.; He, T.; Lotz, B. *Phys. Rev. Lett.* **1999**, *83*, 4558−4561.
(6) Hulvat, J. F.; Stupp, S. I. *Angew. Chem., Int. Ed.* **2002**, *41*, 1705−1709.
(7) Ungar, G.; Liu, Y.; Zeng, X.; Percec, V.; Cho, W.-D. *Science* **2003**, *299*, 1208−1211.
(8) Thomas, E. L.; Anderson, D. M.; Henkee, C. S.; Hoffman, D. *Nature* **1988**, *334*, 598−601.
(9) Bates, F. S.; Fredrickson, G. H. *Annu. Rev. Phys. Chem.* **1990**, *41*, 525−557.
(10) Ho, R.-M.; Chiang, Y.-W.; Tsai, C.-C.; Lin, C.-C.; Ko, B.-T.; Huang, B.-H. *J. Am. Chem. Soc.* **2004**, *126*, 2704−2705.
(11) Chiang, Y.-W.; Ho, R.-M.; Ko, B.-T.; Lin, C.-C. *Angew. Chem., Int. Ed.* **2005**, *44*, 7969−7972.
(12) Chiang, Y.-W.; Ho, R.-M.; Thomas, E. L.; Burger, C.; Hsiao, B. S. *Adv. Funct. Mater.* **2009**, *19*, 448−459.
(13) Ho, R.-M.; Chiang, Y.-W.; Chen, C.-K.; Wang, H.-W.; Hasegawa, H.; Akasaka, S.; Thomas, E. L.; Burger, C.; Hsiao, B. S. *J. Am. Chem. Soc.* **2009**, *131*, 18533−18542.
(14) Chen, C.-K.; Lin, S.-C.; Chiang, Y.-W.; Ho, R.-M.; Lotz, B. *Macromolecules* **2010**, *43*, 7752−7758.
(15) Chen, C.-K.; Hsueh, H.-Y.; Chiang, Y.-W.; Ho, R.-M.; Akasaka, S.; Hasegawa, H. *Macromolecules* **2010**, *43*, 8637−8644.
(16) Ho, R.-M.; Chiang, Y.-W.; Lin, S.-C.; Chen, C.-K. *Prog. Polym. Sci.* **2011**, *36*, 376−453.
(17) Chiang, Y.-W.; Ho, R.-M.; Burger, C.; Hasegawa, H. *Soft Matter* **2011**, *7*, 9797−9803.
(18) Wang, H.-F.; Wang, H.-W.; Ho, R.-M. *Chem. Commun.* **2012**, *48*, 3665−3667.
(19) Ho, R.-M.; Li, M.-C.; Lin, S.-C.; Wang, H.-F.; Lee, Y.-D.; Hasegawa, H.; Thomas, E. L. *J. Am. Chem. Soc.* **2012**, *134*, 10974−10986.
(20) Yu, T.-L.; Huang, B.-H.; Hung, W.-C.; Lin, C.-C.; Wang, T.-C.; Ho, R.-M. *Polymer* **2007**, *48*, 4401−4411.
(21) Sun, Y.-S.; Chung, T.-M.; Li, Y.-J.; Ho, R.-M.; Ko, B.-T.; Jeng, U.-S.; Lotz, B. *Macromolecules* **2006**, *39*, 5782−5788.
(22) Matsen, M. W.; Bates, F. S. *J. Polym. Sci., Part B: Polym. Phys.* **1997**, *35*, 945−952.
(23) Bollinne, C.; Stone, V. W.; Carlier, V.; Jonas, A. M. *Macromolecules* **1999**, *32*, 4719−4724.
(24) Anderson, K. S.; Hillmyer, M. A. *Macromolecules* **2004**, *37*, 1857−1862.

(25) Kim, G.; Libera, M. *Macromolecules* **1998**, *31*, 2569−2577.